

Quantum-annealing-inspired algorithms for multijet clustering

Hideki Okawa^{a,*}, Xian-Zhe Tao^{b,c,d,e}, Qing-Guo Zeng^{b,c,d,e}, Man-Hong Yung^{b,c,d,e}

^a*Institute of High Energy Physics, Chinese Academy of Sciences, Beijing, 100049, China*

^b*Shenzhen Institute for Quantum Science and Engineering, Southern University of Science and Technology, Shenzhen, 518055, China*

^c*International Quantum Academy, Shenzhen, 518048, China*

^d*Guangdong Provincial Key Laboratory of Quantum Science and Engineering, Southern University of Science and Technology, Shenzhen, 518055, China*

^e*Shenzhen Key Laboratory of Quantum Science and Engineering, Southern University of Science and Technology, Shenzhen, 518055, China*

Abstract

Jet clustering or reconstruction is a crucial component at high energy colliders, a procedure to identify sprays of collimated particles originating from the fragmentation and hadronization of quarks and gluons. It is a complicated combinatorial optimization problem and requires intensive computing resources. In this study, we formulate jet reconstruction as a quadratic unconstrained binary optimization (QUBO) problem and introduce novel quantum-annealing-inspired algorithms for clustering multiple jets in electron-positron collision events. One of these quantum-annealing-inspired algorithms, ballistic simulated bifurcation, overcomes problems previously observed in multijet clustering with quantum-annealing approaches. We find that both the distance defined in the QUBO matrix and the prediction power of the QUBO solvers have crucial impacts on the multijet clustering performance. This study opens up a new approach to globally reconstructing multijet beyond dijet in one go, in contrast to the traditional iterative method.

Keywords: High-energy physics, Jet clustering, Quantum computation, Quantum annealing, Simulated bifurcation

1. Introduction

Jet clustering is a fundamental component at high energy colliders to determine the kinematics of the underlying processes governed by quantum chromodynamics (QCD). Due to color confinement, quarks and gluons produced by the collisions or the decays of heavy particles initiate sprays of collimated particles originating from their fragmentation and hadronization. Jets serve as reliable proxies to determine the original parton kinematics.

Jet reconstruction is a complicated combinatorial optimization problem and requires intensive computing resources. It dates back to the proposal by Sternman and Weinberg [1], and various algorithms have been developed over decades since then, as reviewed in Refs. [2–6]. The majority of widely used jet clustering algorithms are implemented in FASTJET [7] for both hadron and e^+e^- colliders and have successfully been used in various experiments, including those at the Large Hadron Collider (LHC) [8–12].

As we face the unprecedented increase in luminosity at the High-Luminosity LHC (HL-LHC) [13] and future colliders under consideration, such as the Circular Electron Positron Collider (CEPC) [14–16], new approaches are being investigated actively to overcome this challenge. Applications of quantum computing and algorithms have recently attracted much attention, and have been applied to track reconstruction for example [17–25]. It also led to the recent investigations on the jet reconstruction using the quantum annealing (QA) [26–29] and quantum gate machines [30–32].

This work demonstrates the potential of quantum-annealing-inspired algorithms (QAIAs) to pursue multijet clustering. In previous works using quantum annealing [26–28], reconstructing dijet has been pursued either with the thrust- or quantum-angle-based approach, with the latter providing higher performance. However, there was a degradation in performance in multijet reconstruction [28], as multiple qubits are required to implement “one-hot” encoding and are error-prone [33]. By replacing the quantum-angle with the $ee-k_t$ distance in the algorithm and using QAIAs, which will be detailed in Section 2, we overcome the problem and maintain or even slightly improve performance from the traditional methods for the multijet reconstruction. Furthermore, as it is a “quantum-inspired” approach, our algorithms run on classical computers, and thus neither suffer from quantum hardware noise nor the limitations of the data size that it can handle. This study opens up a new approach to globally reconstructing multijet in one go, in contrast to the traditional iterative methods.

2. Methodology

Jet clustering can be regarded as a combinatorial optimization problem, which could be formulated as a quadratic unconstrained binary optimization (QUBO) or Ising problem [34]. The difference between the two lies in using zero/one binaries for the former or the ± 1 spins for the latter. The problem is designed in a way that the ground state of the QUBO/Ising model provides the correct answer. It is an NP (Nondeterministic Polynomial time) complete problem, and the solution candidates diverge exponentially with the problem size. Quantum

*Corresponding author

Email address: okawa@ihep.ac.cn (Hideki Okawa)

annealing (QA) machines by D-Wave based on the concept described in Ref. [35] and the coherent Ising machine (CIM) [36] are developed to efficiently solve such kinds of problems, for example. However, QA generally provides suboptimal results when handling largely connected graphs due to the limited connectivity of qubits and hardware noise [37–40]. Such a trend is consistently observed in the previous jet clustering studies [26, 27]. In this study, we introduce simulated bifurcation (SB), which overcomes those challenges.

2.1. Simulated bifurcation

The SB algorithm [41] emulates the quantum bifurcation machine (QbM) [42, 43]. It solves combinatorial optimization problems through quantum adiabatic evolution of Kerr-nonlinear parametric oscillators, exhibiting bifurcation phenomena to represent the two Ising spin states. SB can update all the spins of the Ising problem in parallel, which allows us to achieve computational acceleration. As stated above, solving the Ising problem is to find a spin configuration $\{x_i\}_{i=1}^N \in \{-1, 1\}^N$ that minimizes the Hamiltonian of the Ising model:

$$H(x_i) = \frac{1}{2} \sum_{ij} J_{ij} x_i x_j + \sum_i h_i x_i. \quad (1)$$

In QbM, the Ising model is coupled to the Kerr-nonlinear parametric oscillators. According to the adiabatic evolution theory, if we set the initial state to the ground state of the system and the Hamiltonian changes gradually, the system will remain in the ground state throughout the evolution. Thus, in the end, we can obtain the ground state of the Ising problem. The corresponding classical analog, classical bifurcation machines (CbM) [42, 43], are derived by approximating the expectation value of annihilation operator with a complex amplitude $x_i + iy_i$. x_i and y_i are, respectively, the position and momentum of the i -th Kerr-nonlinear oscillator corresponding to the i -th spin. The original version of SB, adiabatic SB (aSB) [41], simplifies and improves CbM but is prone to errors originating from the continuous treatment of the spins in the differential equations. Two variants of SB are introduced to suppress such analog errors: ballistic SB (bSB) and discrete SB (dSB) [44]. The former introduces inelastic walls at $x_i = \pm 1$ as follows:

$$\dot{x}_i = \frac{\partial H_{\text{bSB}}}{\partial y_i} = a_0 y_i \quad (2)$$

$$\begin{aligned} \dot{y}_i &= -\frac{\partial H_{\text{bSB}}}{\partial x_i}, \\ &= -[a_0 - a(t)] x_i + c_0 \left(h_i + \sum_{j=1}^N J_{ij} x_j \right), \end{aligned} \quad (3)$$

$$H_{\text{bSB}} = \frac{a_0}{2} \sum_{i=1}^N y_i^2 + V_{\text{aSB}} \quad (4)$$

$$V_{\text{bSB}} = \begin{cases} \frac{a_0 - a(t)}{2} \sum_{i=1}^N x_i^2 - c_0 \left(\frac{1}{2} \sum_{i,j} J_{ij} x_i x_j + \sum_i h_i x_i \right), \\ \forall x_i, |x_i| \leq 1 \\ \infty, \text{ otherwise} \end{cases} \quad (5)$$

where a_0 and c_0 are positive constants (the detuning frequency for the former and the coupling strength for the latter), $a(t)$ is a time-dependent pumping amplitude that monotonically increases from zero to a_0 , H_{bSB} is the Hamiltonian, and V_{bSB} is the potential energy in bSB.

To further suppress the error from continuous relaxation of x_i , dSB discretizes x_j to $\text{sgn}(x_j)$ in the mean-field term:

$$\dot{x}_i = \frac{\partial H_{\text{dSB}}}{\partial y_i} = a_0 y_i \quad (6)$$

$$\dot{y}_i = \frac{\partial H_{\text{dSB}}}{\partial x_i} = -[a_0 - a(t)] x_i + c_0 \left(\sum_{j=1}^N J_{ij} \text{sgn}(x_j) + h_i \right) \quad (7)$$

$$H_{\text{dSB}} = \frac{a_0}{2} \sum_{i=1}^N y_i^2 + V_{\text{dSB}} \quad (8)$$

$$V_{\text{dSB}} = \begin{cases} \frac{a_0 - a(t)}{2} \sum_{i=1}^N x_i^2 - c_0 \left(\frac{1}{2} \sum_{i,j} J_{ij} x_i \text{sgn}(x_j) + \sum_j h_j x_j \right), \\ \forall x_i, |x_i| \leq 1 \\ \infty, \text{ otherwise} \end{cases} \quad (9)$$

Finally, the $\text{sgn}(x_i)$ gives the solution of the Ising problem. For all the SB variants, the symplectic Euler method is adopted for the numerical computation [45].

The SB algorithms used in this study are implemented in Huawei MindSpore Quantum [46, 47]. A simulated annealing library, D-Wave Neal [48], is adopted as a benchmark for comparing to the SB algorithms.

2.2. Jet reconstruction as an Ising problem

As proposed in Refs. [26–28] jet reconstruction can be formulated in terms of a QUBO Hamiltonian:

$$O_{\text{QUBO}}(s_i) = \sum_{i,j=1}^{N_{\text{input}}} Q_{ij} s_i s_j, \quad (10)$$

where s_i is the binary $\{0,1\}$ for each jet constituent to define which jet it is assigned to, Q_{ij} is the QUBO matrix, which stores the distance between the i -th and j -th constituents, and N_{input} is the number of inputs, namely the jet constituents. A QUBO Hamiltonian can be converted to an Ising Hamiltonian (Eq.1) by:

$$x_i \longleftrightarrow 2s_i - 1 \quad (11)$$

$$J_{ij} \longleftrightarrow \frac{Q_{ij}}{2} \quad (12)$$

$$h_i \longleftrightarrow \frac{\sum_j Q_{ij}}{2}. \quad (13)$$

The thrust and quantum angle-based algorithms were considered in the previous studies [26–28]. In this study, the quantum angle-based algorithm is considered as a benchmark and its QUBO matrix is defined as:

$$Q_{ij} = -\frac{\vec{p}_i \cdot \vec{p}_j}{2(|\vec{p}_i| \cdot |\vec{p}_j|)}, \quad (14)$$

where \vec{p}_i is the momentum of the i -th jet constituent. It is compared to the QUBO matrix based on the ee - k_t distance [49]:

$$Q_{ij} = 2\min(E_i^2, E_j^2)(1 - \cos \theta_{ij}), \quad (15)$$

where E_i is the energy of the i -th jet constituent and θ_{ij} is the angle between the i -th and j -th jet constituents. The ee - k_t or the so-called Durham algorithm [49] is the standard jet-finding algorithm adopted in recent electron-positron colliders and is described in Section 2.3.

It is worth noting that the above formalism can only handle dijet clustering, as is evident from the binary implementation. In order to expand the method to multijet problems, the QUBO can be generalized to [26, 28]:

$$O_{\text{QUBO}}^{\text{multijet}}(s_i^{(n)}) = \sum_{n=1}^{n_{\text{jet}}} \sum_{i,j=1}^{N_{\text{input}}} Q_{ij} s_i^{(n)} s_j^{(n)} + \lambda \sum_{i=1}^{N_{\text{input}}} \left(1 - \sum_{n=1}^{n_{\text{jet}}} s_i^{(n)} \right)^2, \quad (16)$$

where n considers the jet multiplicity and the binary $s_i^{(n)}$ is defined for each jet. The second term is introduced as the constraint to ensure that each jet constituent is assigned to a jet only once. The coefficient of this penalty λ must be large enough: $\lambda > N_{\text{input}} \max_{i,j} Q_{ij}$ [26]. In this study, the jet multiplicity is fixed to a certain value, as is the case for the exclusive jet finding pursued at the electron-positron colliders.

2.3. Benchmark algorithm

The Durham, or ee - k_t algorithm, is adopted as our benchmark since it is the standard jet finder at the electron-positron colliders. It is implemented in the FASTJET software package [7]. The algorithm computes the distance d_{ij} between every pair of inputs i and j :

$$d_{ij} = 2\min(E_i^2, E_j^2)(1 - \cos \theta_{ij}). \quad (17)$$

It iteratively loops over and finds the smallest d_{ij} and recombines the two inputs into a single ‘‘particle.’’ The exclusive mode, which we consider in this study, terminates when the iteration reaches a fixed number of jets manually defined by the user. For the inclusive mode, usually adopted at hadron colliders, the user defines a scale d_{cut} , and the iteration stops when the minimum d_{ij} exceeds the threshold. This study does not consider the latter since we only analyze the electron-positron collision events.

3. Dataset and event selection

We generate Monte Carlo (MC) simulated datasets for three physics processes, $e^+e^- \rightarrow Z \rightarrow q\bar{q}$, $e^+e^- \rightarrow ZH \rightarrow q\bar{q}b\bar{b}$ and $e^+e^- \rightarrow t\bar{t} \rightarrow bq\bar{q}'\bar{b}\bar{q}''q'''$ at the center-of-mass energy of 91 GeV, 240 GeV and 350 GeV respectively, with MADGRAPH_AMC@NLO [50] for the matrix element calculation, PYTHIA8 [51] (v8.2, GPL-2) for the parton showering and hadronization, and DELPHES [52] (v3.4.2, GPL-3) using the fourth detector concept [53] from the Circular Electron Positron Collider (CEPC), a future Higgs boson factory under consideration in China, for the fast simulation of detector effects. The

Particle Flow (EFlow) objects are considered as the jet reconstruction input. The three scenarios of the center-of-mass energy are in accordance with the CEPC proposal and are adopted here to evaluate the reconstruction performance for various jet multiplicities.

We only select events in which all the jets are within the detector acceptance, namely $|\cos \theta| < 0.9$. Furthermore, the separations of two jets with the lowest transverse momenta in the events (n -th and m -th jets):

$$\sqrt{d_{nm}^{(\text{jet})}} = \sqrt{2\min(E_n^{(\text{jet})2}, E_m^{(\text{jet})2})(1 - \cos \theta_{nm})}, \quad (18)$$

are required to be larger than 20 GeV. This selection significantly suppresses background with QCD (gluon) radiation with a minimal impact on the signal [54] and is adopted as a baseline pre-selection in this study. In the ZH and $t\bar{t}$ events, we require them to have exactly two b -tagged jets. To simplify the analysis mentioned in Section 4, only the ZH events with the Z bosons decaying to non- b quarks are generated in the above MC simulation sample.

4. Results

In order to pursue jet clustering, QUBO Hamiltonians (Eq. 16) are defined on an event-by-event basis. The jet multiplicity n_{jet} is set to 2, 4, and 6, respectively, for the Z boson, ZH , and $t\bar{t}$ production events. The binary $s_i^{(n)}$ for each jet constituent from the predicted ground state tells us whether the jet constituent is assigned to the n -th jet. Thus, the precision of the ground state prediction is the key to reconstructing the jets successfully.

First, the predicted minimum energy for Eq. 16 by the three QAIAAs are presented in Figure 1 for a specific event from the three physics processes and two QUBO matrix definitions (Eqs. 14 and 15) as examples. For all cases, bSB outperforms dSB and D-Wave Neal, i.e. in terms of the mean predicted energy and stability against multiple measurements. The trend becomes increasingly apparent as the physics process becomes more complicated, leading to an order-of-magnitude improvement in the minimum energy prediction for the $t\bar{t}$ process using the ee - k_t distance. dSB, on the other hand, fails to predict minimum energy, and its performance is often comparable to that of D-Wave Neal. It is worth noting that the QUBO matrices for jet reconstruction are generally fully-connected matrices unlike the sparse QUBOs defined in track reconstruction [17–23]. QA is known for degraded performance in such a fully-connected case [27], and, remarkably, bSB can still provide quasi-optimal solutions.

In order to evaluate the performance of jet clustering algorithms, the most naive approach would be to compare with the true assignment of constituents to a jet corresponding to the original parton. However, as also stated in Ref. [31], it is not possible to define such an assignment in a reasonable manner. The fundamental issue is that the final state hadrons are occasionally hadronized from quarks originating from different initial partons. The situation will be even more complicated and

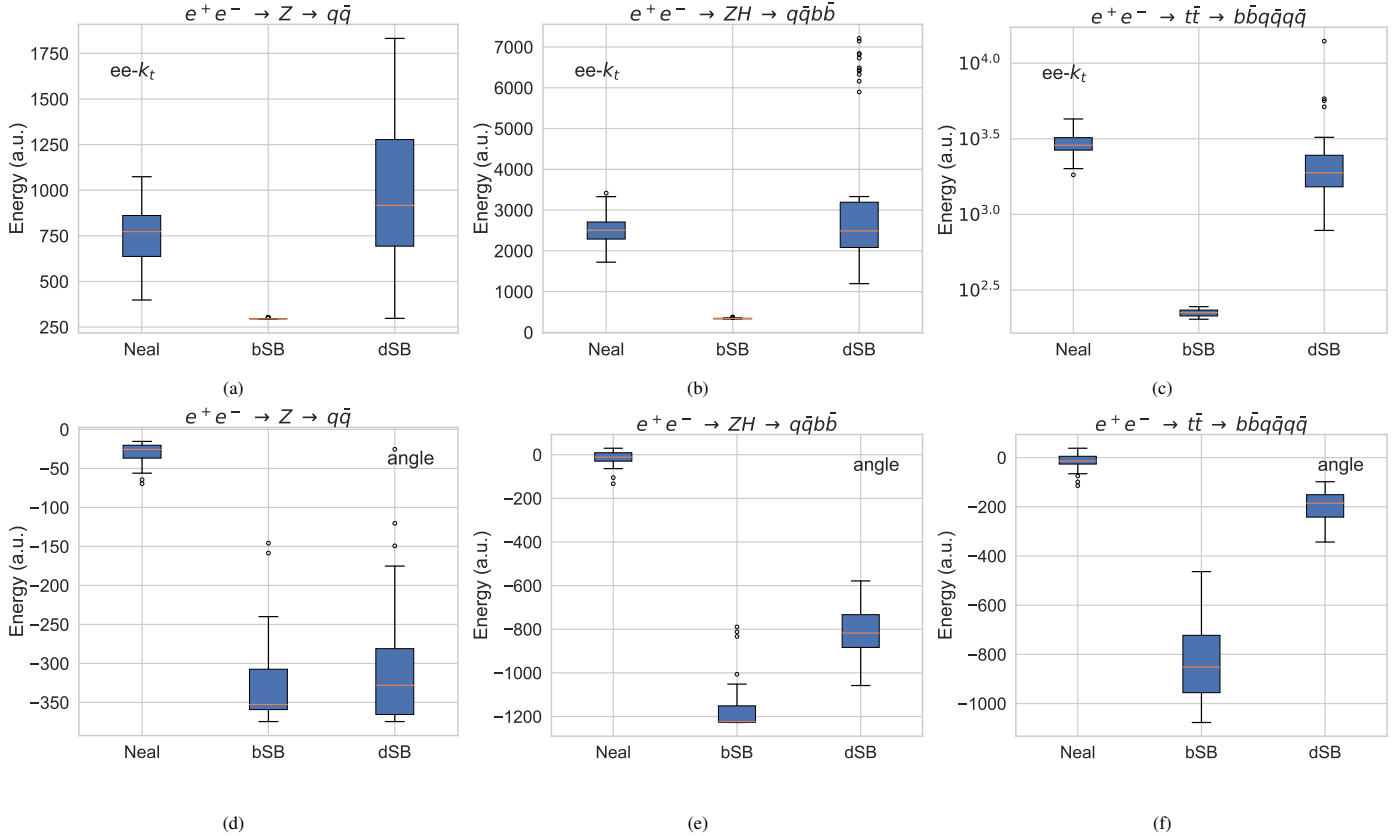


Figure 1: Minimum Ising energies by the three QAIAs for a Z boson (a,d), ZH (b,e), and $t\bar{t}$ events (c,f) with the $ee-k_t$ -based (a,b,c) or angle-based (d,e,f) distance considered in the QUBO formulation.

fundamentally ambiguous when high-order calculations come into play. Thus, it is impossible to define the “true” parton association in a meaningful way.

We adopt a commonly taken approach [28, 31] to define a jet-constituent matching “efficiency” per jet by comparing to a corresponding classical algorithm, $ee-k_t$ implemented in FASTJET, and quantify the percentage of the jet constituents clustered in the same way:

$$\epsilon_{\text{jet}} = \frac{\# \text{ of constituents clustered the same as FASTJET}}{\# \text{ of constituents from FASTJET } ee-k_t}. \quad (19)$$

In the actual computation, the QAIA returns outputs of n_{jet} arrays of jet constituent indices, where each array represents a jet. The jets reconstructed by FASTJET are recorded in the same manner to compute the efficiency. The number of overlapping array components between FASTJET and the QAIA are used for the numerator in Eq. 19.

Figure 2 shows event displays from a $t\bar{t}$ event using the benchmark $ee-k_t$ algorithm implemented in FASTJET and three QAIA using the $ee-k_t$ -distanced QUBO. The jet constituents are represented as circles with their size being proportional to their energy. The colors represent the individual jets. Event displays with the angle-based QUBO, as well as for the other two physics processes, are presented in Appendix A. It is clearly seen that only bSB with the $ee-k_t$ -distanced QUBO can successfully reconstruct jets for all three physics processes. For

low-energy jet constituent outliers, FASTJET and bSB occasionally assigns them to different jets. Their impact is evaluated later in terms of invariant mass resolution.

Figure 3 shows the jet efficiencies (Eq. 19) evaluated for the three physics processes using the three QAIA with two types of QUBOs: $ee-k_t$ -based (Eq. 15) and angle-based (Eq. 14). Several important findings can be seen from the figures. First, the $ee-k_t$ -based approach outperforms the angle-based counterpart for all the physics processes. This is partially expected due to the consistent definition of the distance in the $ee-k_t$ -based QUBO. More importantly, the angle-based QUBO stops functioning for jet multiplicities beyond two; the jet efficiency largely degrades in the ZH and $t\bar{t}$ events, and even some jets have zero efficiency, meaning that they fail to be reconstructed despite the requirement of exclusive jet reconstruction. Most important of all, only bSB remains to succeed in jet reconstruction for all three physics processes. With dSB and D-Wave Neal, the constituents are often chaotically and unreasonably assigned to a jet, as can be seen in Figures 2, A.6, A.7, and A.8. As stated above, fully-connected QUBOs are notoriously challenging to predict the minimum energy. bSB significantly outperforms dSB and Neal in this regard and demonstrates itself as a promising QUBO problem solver for handling multijet reconstruction.

As the benchmark $ee-k_t$ algorithm implemented in FASTJET does not necessarily provide the exact “correct” answer, the jet

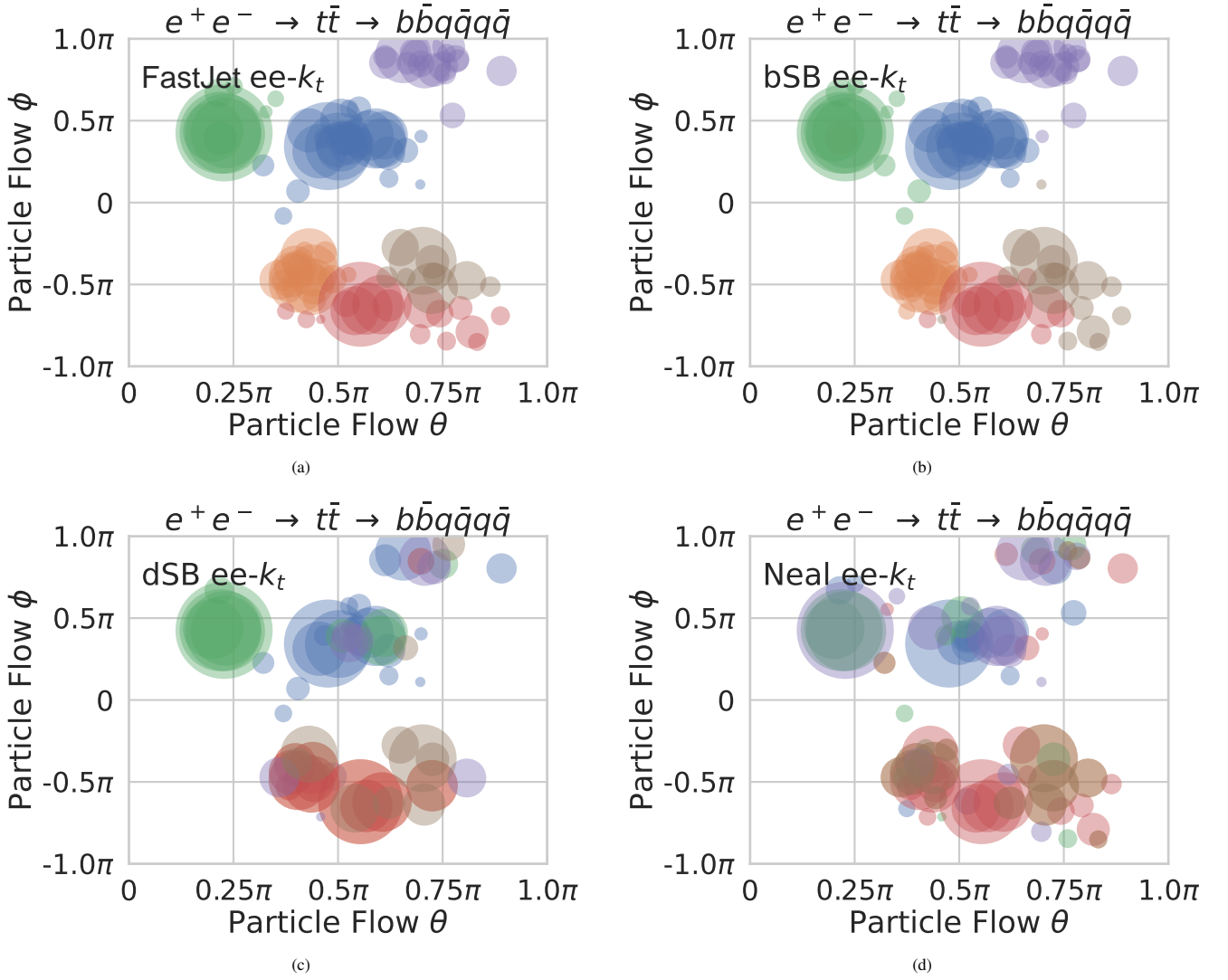


Figure 2: Event displays from a $t\bar{t}$ event with jet reconstructed by (a) $ee-k_t$ algorithm implemented in FASTJET or with the $ee-k_t$ -distanced QUBO approach using (b) bSB, (c) dSB or (d) D-Wave Neal. Each circle represents a particle flow candidate with its size proportional to the energy. Each color corresponds to an individual jet.

efficiency alone does not give us a fully decisive picture on the overall jet reconstruction performance. To evaluate the impact on the actual physics analysis, the invariant masses of the Z , Higgs bosons and top quarks are presented in Figure 4. In the ZH events, the two b -tagged jets are assumed to originate from the Higgs bosons and are used in the mass reconstruction. The top-quark mass reconstruction is pursued in two steps as was done in Ref. [55]: the two b -jets are assumed to originate from the b -quarks, and the light-flavor jet pairs with the least deviation from the W -boson mass m_W are selected from the three possible permutations:

$$|m_{ij} - m_W| + |m_{kl} - m_W|, \quad (20)$$

where i, j, k, l are the jet indices. Then, one of the two possible combinations of these light-flavor jet pairs and the b -jets that are more compatible with the top-quark mass is adopted. We did not consider the χ^2 method [56], kinematic likelihood [57],

or state-of-the-art machine learning methods [58–63] usually applied in hadron colliders, as the event topology and our assumption are simpler; the jet multiplicity is fixed to six, and the b -jets are assumed to come from the b -quarks.

FASTJET and bSB provide comparable performance in the Z boson events, but dSB and D-Wave Neal already show visibly degraded mass resolution. In the ZH and $t\bar{t}$ events, dSB and D-Wave Neal fail to reconstruct the jets in a reasonable manner as described above and are not shown in the figure. For these high-jet-multiplicity events (Figure 4b,4c), bSB provides slightly better mass resolution than the baseline FASTJET $ee-k_t$. The results indicate that the global QUBO jet reconstruction using bSB may provide more precise clustering.

The execution time for each QAIA algorithm is evaluated on an AMD Ryzen 7 6800HS Creator Edition CPU and an NVIDIA A100 GPU. Figure 5 presents the evolution of Ising energies and jet efficiencies evaluated for the three QAIAs. We

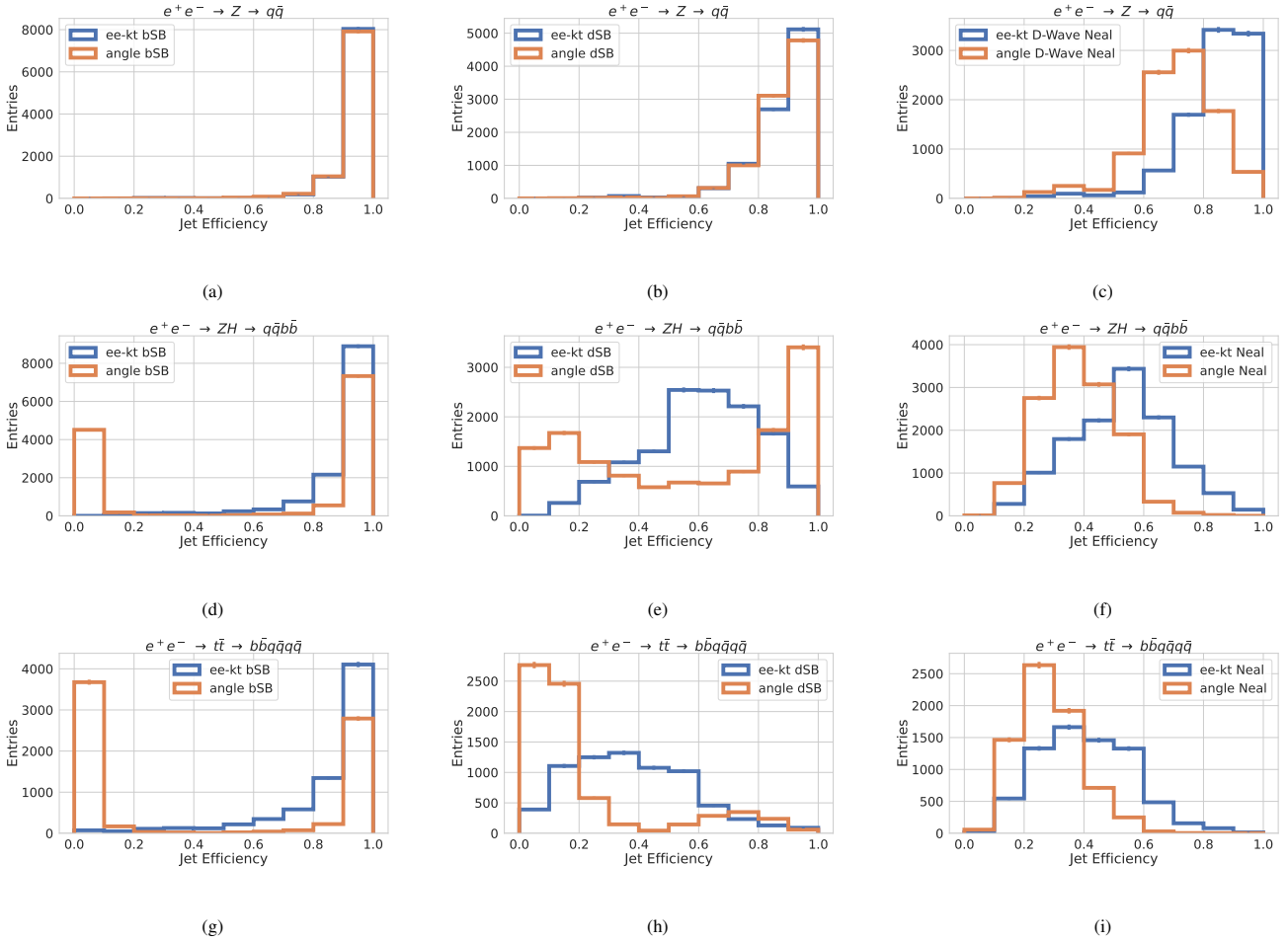


Figure 3: Constituent-matching efficiencies to FASTJET for jets reconstructed by bSB (a,d,g), dSB (b,e,h), and D-Wave Neal (c,f,i) using ee - k_t or angle-based QUBOs.

control the total runtime of the algorithms by setting different numbers of iterations. Only one CPU or GPU is used for fair comparison with D-Wave Neal. The average of the 100 (50) shots for the Z boson (ZH and $t\bar{t}$) events and the envelopes defined from the standard deviation from the mean are shown in the figure. bSB performs the best and rapidly converges to optimal values, whereas dSB and D-Wave Neal fail to reach reasonable jet efficiencies and Ising energies regardless of the running time.

5. Conclusion and Outlook

In our study, jet clustering is formulated as a QUBO problem. Three QAIAs are adopted to pursue global reconstruction, which is a new approach compared to the traditional iterative reconstruction, implemented in FASTJET. The distance defined in the QUBO design significantly impacts the reconstruction performance, particularly when the jet multiplicity is beyond two. We find that the angle-based approach only provides reasonable performance for dijet events, and alternative distances such as ee - k_t are mandatory for higher jet multiplicities. For such multijet cases, it becomes exceedingly difficult even to approximately search for the “quasi”-ground state, ending up in

a local minimum, which has an order-of-magnitude higher energy than the optimal states (Figure 1b, 1c). Because of such a challenge, previous studies saw fairly degraded performance in multijet reconstruction. However, this study shows that a powerful QUBO problem solver, bSB among the three QAIAs, can find optimal solutions. It demonstrates its outstanding capability to solve combinatorial optimization problems despite the high QUBO connectivities. It is promising that this global jet reconstruction with bSB can improve the invariant mass reconstruction in multijet events.

As a “quantum-inspired” algorithm, bSB runs on classical computers and is suitable for parallel processing and using cutting-edge computing resources such as GPUs and FPGAs. It is important to note that we can flexibly balance speed and reconstruction precision in QAIAs. Namely, if precise energy resolution is not required for low-level triggers, for example, we can run the reconstruction much faster. Thus, with the applicability to run on FPGAs, bSB may particularly provide an important option to be considered for triggers during the Z-pole data taking at the CEPC, an “exabyte”-level data taking comparable to the intensive HL-LHC conditions. The running time tends to be longer for high jet multiplicity events, and further investigations on the speed-up are ongoing.

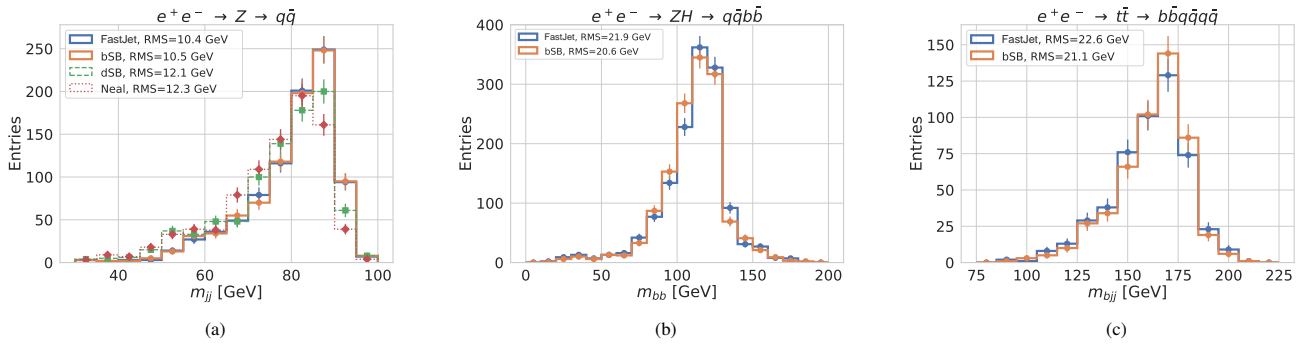


Figure 4: Invariant masses of Z bosons (a), Higgs bosons (b), and top quarks (c) with jets reconstructed by FASTJET and QAIAs. Only FASTJET and bSB are shown in (b,c), as dSB and Neal provide largely degraded performance and even fail to reconstruct some jets in the events.

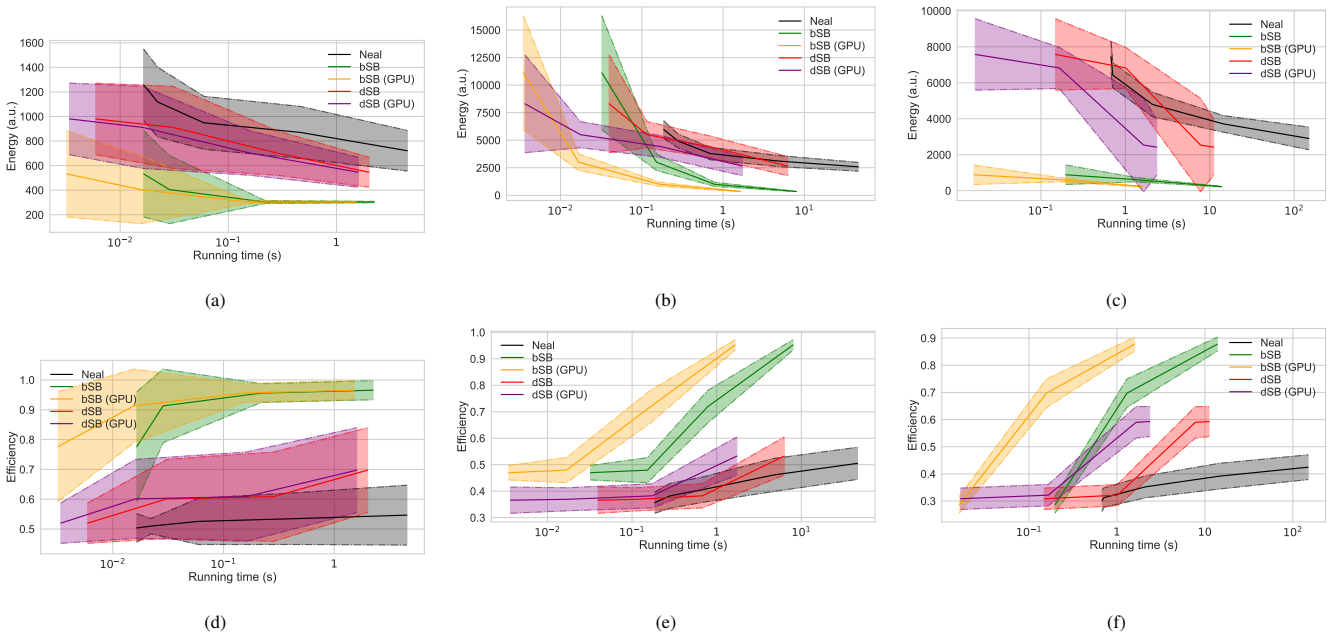


Figure 5: Evolution of Ising energies (a,b,c) and jet efficiencies (d,e,f) against the running time from the three QAIAs presented for (a,d) Z boson, (b,e) ZH, and (c,f) $t\bar{t}$ events. The $ee-k_t$ distance is adopted in the QUBO formulation. The solid lines are the average of multiple shots (100 for Z and 50 for ZH and $t\bar{t}$), and the envelopes represent the standard deviation from the mean of those shots.

Lastly, this study concentrates on e^+e^- collider conditions and exclusive jet reconstruction, but an extension to inclusive jet reconstruction at hadron colliders would also be of interest and is left for future studies.

Acknowledgments

HO would like to thank Gang Li, Shudong Wang, and Xu Gao for their feedback regarding the CEPC 4th detector concept in Delphes. HO is supported by the National Natural Science Foundation of China (NSFC) under Grant No. 12075060 and the NSFC Basic Science Center Program for Joint Research on High Energy Frontier Particle Physics under Grant No. 12188102.

Appendix A. Event displays

Figures A.6-A.8 present event displays for the three physics processes reconstructed with the benchmark FASTJET $ee-k_t$ algorithm or the bSB, dSB and D-Wave Neal using the $ee-k_t$ or the angled-based QUBOs.

References

- [1] G. F. Sterman, S. Weinberg, Jets from Quantum Chromodynamics, *Phys. Rev. Lett.* 39 (1977) 1436. doi:10.1103/PhysRevLett.39.1436.
- [2] S. Moretti, L. Lonnblad, T. Sjostrand, New and old jet clustering algorithms for electron - positron events, *JHEP* 08 (1998) 001. doi:10.1088/1126-6708/1998/08/001.
- [3] G. C. Blazey, et al., Run II jet physics, in: *Physics at Run II: QCD and Weak Boson Physics Workshop: Final General Meeting, 2000*, pp. 47–77. arXiv:hep-ex/0005012.
- [4] S. D. Ellis, J. Huston, K. Hatakeyama, P. Loch, M. Tonnesmann, Jets in hadron-hadron collisions, *Prog. Part. Nucl. Phys.* 60 (2008) 484–551. doi:10.1016/j.pnpnp.2007.12.002.

- [5] G. P. Salam, Towards Jetography, *Eur. Phys. J. C* 67 (2010) 637–686. doi:10.1140/epjc/s10052-010-1314-6.
- [6] A. Ali, G. Kramer, Jets and QCD: A Historical Review of the Discovery of the Quark and Gluon Jets and its Impact on QCD, *Eur. Phys. J. H* 36 (2011) 245–326. doi:10.1140/epjh/e2011-10047-1.
- [7] M. Cacciari, G. P. Salam, G. Soyez, FastJet User Manual, *Eur. Phys. J. C* 72 (2012) 1896. doi:10.1140/epjc/s10052-012-1896-2.
- [8] LHC Machine, JINST 3 (2008) S08001. doi:10.1088/1748-0221/3/08/S08001.
- [9] G. Aad, et al., The ATLAS Experiment at the CERN Large Hadron Collider, JINST 3 (2008) S08003. doi:10.1088/1748-0221/3/08/S08003.
- [10] S. Chatrchyan, et al., The CMS Experiment at the CERN LHC, JINST 3 (2008) S08004. doi:10.1088/1748-0221/3/08/S08004.
- [11] A. A. Alves, Jr., et al., The LHCb Detector at the LHC, JINST 3 (2008) S08005. doi:10.1088/1748-0221/3/08/S08005.
- [12] K. Aamodt, et al., The ALICE experiment at the CERN LHC, JINST 3 (2008) S08002. doi:10.1088/1748-0221/3/08/S08002.
- [13] I. Béjar Alonso, O. Brüning, P. Fessia, M. Lamont, L. Rossi, L. Taviani, M. Zerlauth (editors), High-Luminosity Large Hadron Collider (HL-LHC): Technical design report, CERN Yellow Reports: Monographs, CERN, Geneva, 2020. doi:10.23731/CYRM-2020-0010.
- [14] W. Abdallah, et al., CEPC Technical Design Report: Accelerator, Radiat. Detect. Technol. Methods 8 (1) (2024) 1–1105. doi:10.1007/s41605-024-00463-y.
- [15] CEPC Study Group, CEPC Conceptual Design Report: Volume 1 - Accelerator, IHEP-CEPC-DR-2018-01, IHEP-AC-2018-01arXiv:1809.00285.
- [16] CEPC Study Group, CEPC Conceptual Design Report: Volume 2 - Physics & Detector, IHEP-CEPC-DR-2018-02, IHEP-EP-2018-01, IHEP-TH-2018-01arXiv:1811.10545.
- [17] F. Bapst, W. Bhimji, P. Calafura, H. Gray, W. Lavrijsen, L. Linder, A pattern recognition algorithm for quantum annealers, *Comput. Softw. Big Sci.* 4 (1) (2020) 1. doi:10.1007/s41781-019-0032-5.
- [18] A. Zlokapa, A. Anand, J.-R. Vlimant, J. M. Duarte, J. Job, D. Lidar, M. Spiropulu, Charged particle tracking with quantum annealing-inspired optimization, *Quantum Machine Intelligence* 3 (2021) 27. doi:10.1007/s42484-021-00054-w.
- [19] L. Funcke, T. Hartung, B. Heinemann, K. Jansen, A. Kropf, S. Kühn, F. Meloni, D. Spataro, C. Tüysüz, Y. C. Yap, Studying quantum algorithms for particle track reconstruction in the LUXE experiment, *J. Phys. Conf. Ser.* 2438 (1) (2023) 012127. doi:10.1088/1742-6596/2438/1/012127.
- [20] A. Crippa, et al., Quantum algorithms for charged particle track reconstruction in the LUXE experiment, DESY-23-045, MIT-CTP/5481, arXiv:2304.01690arXiv:2304.01690.
- [21] T. Schwägerl, C. Issever, K. Jansen, T. J. Khoo, S. Kühn, C. Tüysüz, H. Weber, Particle track reconstruction with noisy intermediate-scale quantum computersarXiv:2303.13249.
- [22] H. Okawa, Charged particle reconstruction for future high energy colliders with quantum approximate optimization algorithm, *Springer Communications in Computer and Information Science* 2036 (2024) 272–283. doi:https://doi.org/10.1007/978-981-97-0065-3_21.
- [23] H. Okawa, Q.-G. Zeng, X.-Z. Tao, M.-H. Yung, Quantum-Annealing-Inspired Algorithms for Track Reconstruction at High-Energy Colliders, *Comput. Softw. Big Sci.* 8 (1) (2024) 16. doi:10.1007/s41781-024-00126-z.
- [24] D. Nicotra, M. Lucio Martinez, J. A. de Vries, M. Merk, K. Driessens, R. L. Westra, D. Dibenedetto, D. H. Cámpora Pérez, A quantum algorithm for track reconstruction in the LHCb vertex detector, JINST 18 (11) (2023) P11028. doi:10.1088/1748-0221/18/11/P11028.
- [25] C. Brown, M. Spannowsky, A. Tapper, S. Williams, I. Xioidis, Quantum pathways for charged track finding in high-energy collisions, *Front. Artif. Intell.* 7 (2024) 1339785. doi:10.3389/frai.2024.1339785.
- [26] A. Y. Wei, P. Naik, A. W. Harrow, J. Thaler, Quantum algorithms for jet clustering, *Phys. Rev. D* 101 (2020) 094015. doi:10.1103/PhysRevD.101.094015.
- [27] A. Delgado, J. Thaler, Quantum annealing for jet clustering with thrust, *Phys. Rev. D* 106 (2022) 094016. doi:10.1103/PhysRevD.106.094016.
- [28] D. Pires, Y. Omar, J. Seixas, Adiabatic quantum algorithm for multijet clustering in high energy physics, *Physics Letters B* 843 (2023) 138000. doi:https://doi.org/10.1016/j.physletb.2023.138000.
- [29] M. Kim, P. Ko, J. hyeon Park, M. Park, Leveraging quantum annealer to identify an event-topology at high energy collidersarXiv:2111.07806.
- [30] J. J. Martínez de Lejarza, L. Cieri, G. Rodrigo, Quantum clustering and jet reconstruction at the Lhc, *Phys. Rev. D* 106 (2022) 036021. doi:10.1103/PhysRevD.106.036021.
- [31] D. Pires, P. Bargassa, J. Seixas, Y. Omar, A digital quantum algorithm for jet clustering in high-energy physicsarXiv:2101.05618.
- [32] Y. Zhu, W. Zhuang, C. Qian, Y. Ma, D. E. Liu, M. Ruan, C. Zhou, A Novel Quantum Realization of Jet Clustering in High-Energy Physics ExperimentsarXiv:2407.09056.
- [33] V. Kumar, G. Bass, C. Tomlin, J. Dulny, Quantum annealing for combinatorial clustering, *Quant. Inf. Proc.* 17 (2) (2018) 39. doi:10.1007/s11128-017-1809-2.
- [34] A. Lucas, Ising formulations of many NP problems, *Front. in Phys.* 2 (2014) 5. doi:10.3389/fphy.2014.00005.
- [35] T. Kadowaki, H. Nishimori, Quantum annealing in the transverse Ising model, *Phys. Rev. E* 58 (1998) 5355–5363. doi:10.1103/PhysRevE.58.5355.
- [36] Z. Wang, A. Marandi, K. Wen, R. L. Byer, Y. Yamamoto, Coherent Ising machine based on degenerate optical parametric oscillators, *Phys. Rev. A* 88 (2013) 063853. doi:10.1103/PhysRevA.88.063853.
- [37] M. W. Johnson, et al., Quantum annealing with manufactured spins, *Nature* 473 (2011) 194–198. doi:10.1038/nature10012.
- [38] P. I. Bunyk, et al., Architectural Considerations in the Design of a Superconducting Quantum Annealing Processor, *IEEE Trans. Appl. Supercond.* 24 (4) (2014) 1700110. doi:10.1109/TASC.2014.2318294.
- [39] S. Boixo, T. F. Rønnow, S. V. Isakov, Z. Wang, D. Wecker, D. A. Lidar, J. M. Martinis, M. Troyer, Evidence for quantum annealing with more than one hundred qubits, *Nature Phys.* 10 (3) (2014) 218–224. doi:10.1038/nphys2900.
- [40] A. S. Boev, S. R. Usmanov, A. M. Semenov, M. M. Ushakova, G. V. Salahov, A. S. Mastiukova, E. O. Kikitenko, A. K. Fedorov, Quantum-inspired optimization for wavelength assignment, *Front. Phys.* 10 (2023) 1092065. doi:10.3389/fphy.2022.1092065.
- [41] H. Goto, K. Tatumura, A. R. Dixon, Combinatorial optimization by simulating adiabatic bifurcations in nonlinear Hamiltonian systems, *Science Advances* 5 (4) (2019) eaav2372. doi:10.1126/sciadv.aav2372.
- [42] H. Goto, Bifurcation-based adiabatic quantum computation with a nonlinear oscillator network, *Sci. Rep.* 6 (1) (2016) 21686. doi:10.1038/srep21686.
- [43] H. Goto, Quantum computation based on quantum adiabatic bifurcations of Kerr-nonlinear parametric oscillators, *Journal of the Physical Society of Japan* 88 (2019) 061015. doi:doi/10.7566/JPSJ.88.061015.
- [44] H. Goto, K. Endo, M. Suzuki, Y. Sakai, T. Kanao, Y. Hamakawa, R. Hidaka, M. Yamasaki, K. Tatumura, High-performance combinatorial optimization based on classical mechanics, *Science Advances* 7 (6) (2021) eabe7953. doi:10.1126/sciadv.abe7953.
- [45] B. Leimkuhler, S. Reich, *Simulating Hamiltonian Dynamics*, Cambridge Monographs on Applied and Computational Mathematics, Cambridge University Press, Cambridge, 2005. doi:https://doi.org/10.1017/CB09780511614118.
- [46] Q.-G. Zeng, X.-P. Cui, B. Liu, Y. Wang, P. Mosharev, M.-H. Yung, Performance of quantum annealing inspired algorithms for combinatorial optimization problems, *Commun. Phys.* 7 (1) (2024) 249. doi:10.1038/s42005-024-01705-7.
- [47] https://github.com/mindspore/mindquantum.
- [48] https://docs.ocean.dwavesys.com/projects/neal.
- [49] S. Catani, Y. Dokshitzer, M. Olsson, G. Turnock, B. Webber, New clustering algorithm for multijet cross sections in e+e- annihilation, *Physics Letters B* 269 (3) (1991) 432–438. doi:https://doi.org/10.1016/0370-2693(91)90196-w.
- [50] J. Alwall, R. Frederix, S. Frixione, V. Hirschi, F. Maltoni, O. Mattelaer, H. S. Shao, T. Stelzer, P. Torrielli, M. Zaro, The automated computation of tree-level and next-to-leading order differential cross sections, and their matching to parton shower simulations, *JHEP* 07 (2014) 079. doi:10.1007/JHEP07(2014)079.
- [51] T. Sjöstrand, S. Ask, J. R. Christiansen, R. Corke, N. Desai, P. Ilten, S. Mrenna, S. Prestel, C. O. Rasmussen, P. Z. Skands, An introduction to PYTHIA 8.2, *Comput. Phys. Commun.* 191 (2015) 159–177.

- doi:10.1016/j.cpc.2015.01.024.
- [52] J. de Favereau, C. Delaere, P. Demin, A. Giammanco, V. Lemaitre, A. Mertens, M. Selvaggi, DELPHES 3, A modular framework for fast simulation of a generic collider experiment, *JHEP* 02 (2014) 057. doi:10.1007/JHEP02(2014)057.
 - [53] M.-Y. Liu, W.-D. Li, X.-T. Huang, Y. Zhang, T. Lin, Y. Yuan, Simulation and reconstruction of particle trajectories in the CEPC drift chamber, *Nucl. Sci. Tech.* 35 (8) (2024) 128. doi:10.1007/s41365-024-01497-z.
 - [54] G. Soyez, Reconstructing and using jets at the FCC-ee, FCC-EE QCD PHYSICS MEETING <https://indico.cern.ch/event/1203309/> (10 2022).
 - [55] K. Seidel, F. Simon, M. Tesar, S. Poss, Top quark mass measurements at and above threshold at CLIC, *Eur. Phys. J. C* 73 (8) (2013) 2530. doi:10.1140/epjc/s10052-013-2530-7.
 - [56] S. S. Snyder, Measurement of the Top Quark Mass at D0, Ph.D. thesis, SUNY, Stony Brook (1995). doi:10.2172/1422822.
 - [57] J. Erdmann, S. Guindon, K. Kroeninger, B. Lemmer, O. Nackenhurst, A. Quadt, P. Stolte, A likelihood-based reconstruction algorithm for top-quark pairs and the KLFilter framework, *Nucl. Instrum. Meth. A* 748 (2014) 18–25. doi:10.1016/j.nima.2014.02.029. URL <https://github.com/KLFilter/KLFilter>
 - [58] J. Erdmann, T. Kallage, K. Kröniger, O. Nackenhurst, From the bottom to the top—reconstruction of $t\bar{t}$ events with deep learning, *JINST* 14 (11) (2019) P11015. doi:10.1088/1748-0221/14/11/P11015.
 - [59] M. J. Fenton, A. Shmakov, T.-W. Ho, S.-C. Hsu, D. Whiteson, P. Baldi, Permutationless many-jet event reconstruction with symmetry preserving attention networks, *Phys. Rev. D* 105 (11) (2022) 112008. doi:10.1103/PhysRevD.105.112008.
 - [60] A. Shmakov, M. J. Fenton, T.-W. Ho, S.-C. Hsu, D. Whiteson, P. Baldi, SPANet: Generalized permutationless set assignment for particle physics using symmetry preserving attention, *SciPost Phys.* 12 (2022) 178. doi:10.21468/SciPostPhys.12.5.178.
 - [61] M. J. Fenton, A. Shmakov, H. Okawa, Y. Li, K.-Y. Hsiao, S.-C. Hsu, D. Whiteson, P. Baldi, Reconstruction of unstable heavy particles using deep symmetry-preserving attention networks, *Commun. Phys.* 7 (1) (2024) 139. doi:10.1038/s42005-024-01627-4.
 - [62] S. Qiu, S. Han, X. Ju, B. Nachman, H. Wang, Holistic approach to predicting top quark kinematic properties with the covariant particle transformer, *Phys. Rev. D* 107 (2023) 114029. doi:10.1103/PhysRevD.107.114029.
 - [63] L. Ehrke, J. A. Raine, K. Zoch, M. Guth, T. Golling, Topological reconstruction of particle physics processes using graph neural networks, *Phys. Rev. D* 107 (11) (2023) 116019. doi:10.1103/PhysRevD.107.116019.

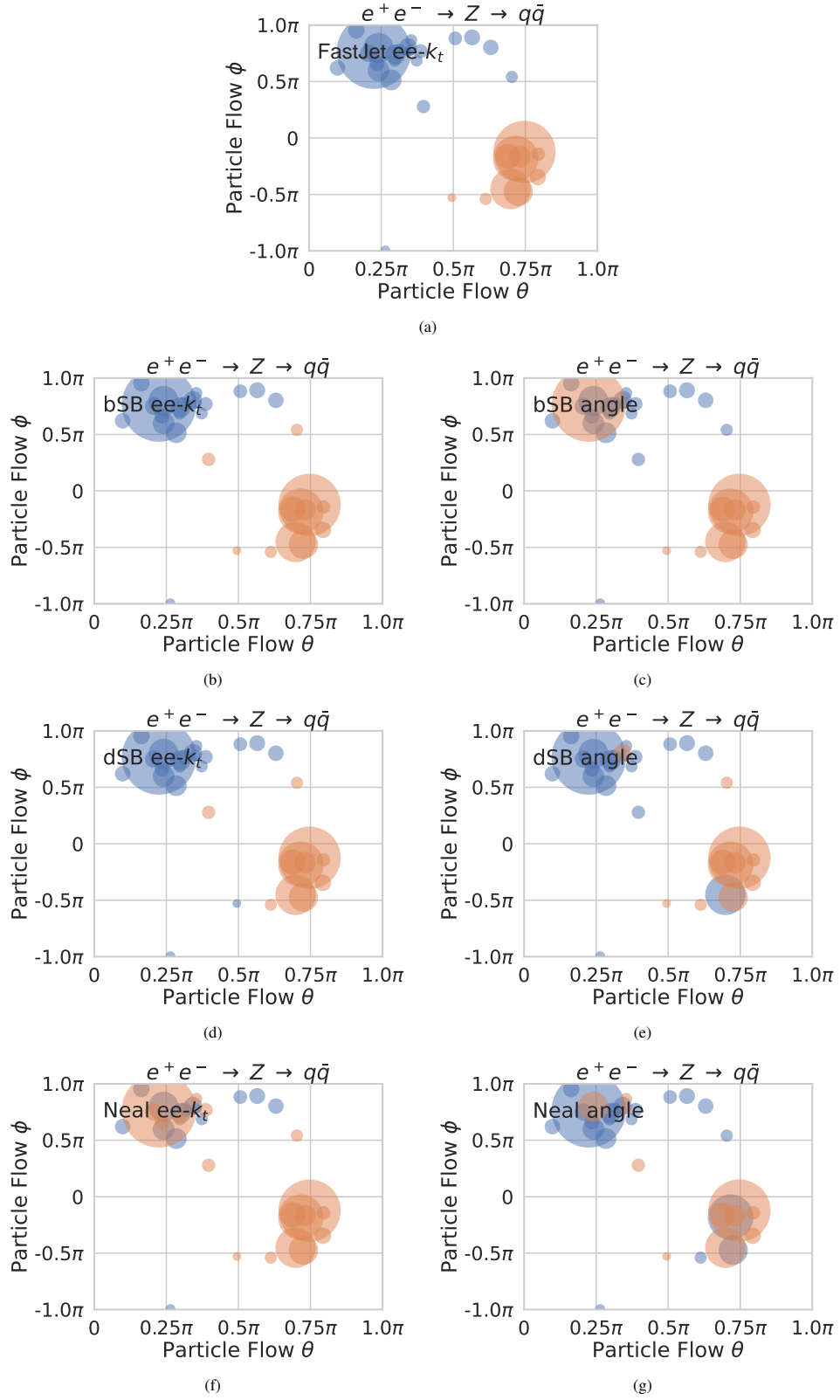


Figure A.6: Event displays from a Z event with jet reconstructed by (a) $ee-k_t$ algorithm implemented in `FASTJET` or with the $ee-k_t$ - or angle-distanced QUBO approach respectively using (b,c) bSB, (d,e) dSB or (e,f) D-Wave Neal. Each circle represents a particle flow candidate with its size proportional to the energy. The same color corresponds to the same jet.

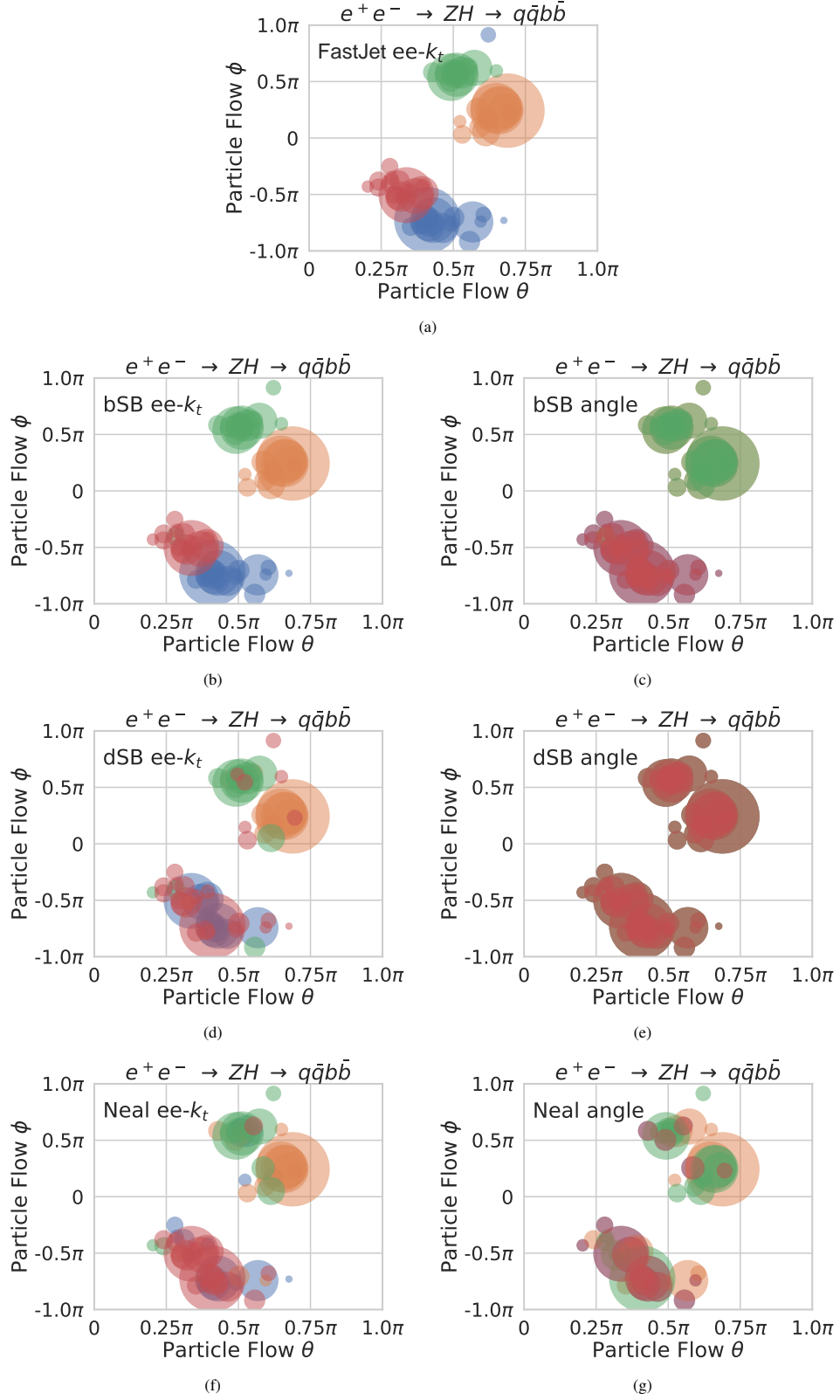


Figure A.7: Event displays from a ZH event with jet reconstructed by (a) $ee-k_t$ algorithm implemented in FASTJET or with the eek_t - or angle-distanced QUBO approach respectively using (b,c) bSB, (d,e) dSB or (e,f) D-Wave Neal. Each circle represents a particle flow candidate with its size proportional to the energy. The same color corresponds to the same jet.

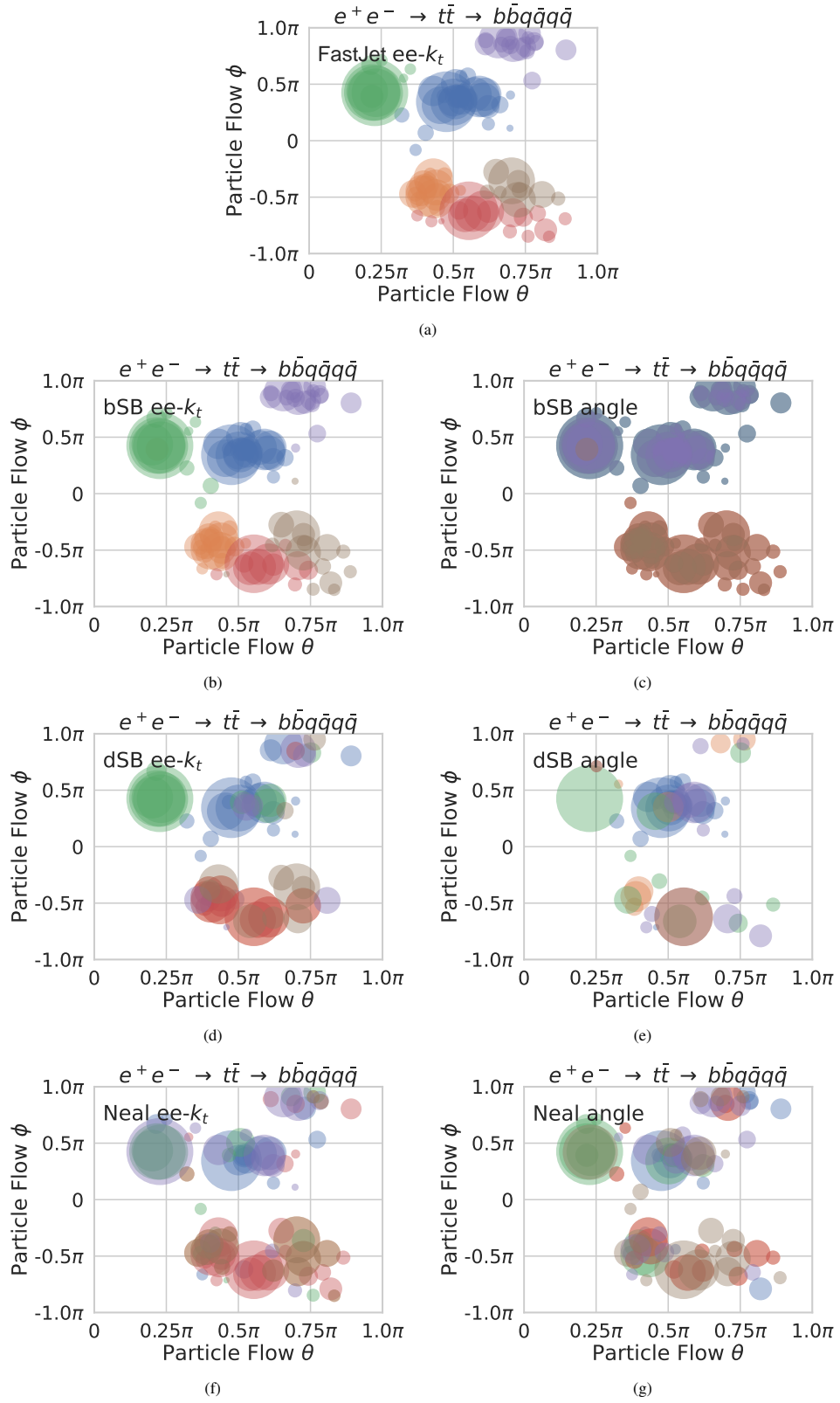


Figure A.8: Event displays from a $t\bar{t}$ event with jet reconstructed by (a) $ee-k_t$ algorithm implemented in FASTJET or with the $ee-k_t$ - or angle-distanced QUBO approach respectively using (b,c) bSB, (d,e) dSB or (e,f) D-Wave Neal. Each circle represents a particle flow candidate with its size proportional to the energy. The same color corresponds to the same jet.